sciendo
ISSN 1335-8871
MEASUREMENT SCIENCE REVIEW
Journal homepage: https://content.sciendo.com

Analysis of Heart Pulse Transmission Parameters Determined from Multi-Channel PPG Signals Acquired by a Wearable Optical Sensor

Jiří Přibil*, Anna Přibilová, Ivan Frollo

Institute of Measurement Science, Slovak Academy of Sciences, Dúbravská cesta 9, 841 04 Bratislava, Slovak Republic, jiri.pribil@savba.sk

Abstract: The article describes the development and testing of a special prototype wearable device consisting of three optical photoplethysmography (PPG) sensors. The functionality of the developed triple PPG sensor was tested under normal laboratory conditions and in a running magnetic resonance imaging (MRI) scanner working with a low magnetic field. The results of the first measurements under normal laboratory conditions show that the obtained mutual positions of systolic/diastolic blood pressure values and heart pulse transmission parameters determined from the PPG waves can be fitted by a line segment with a sufficiently high slope. Measurement experiments inside the open-air MRI tomograph show the practical influence of vibrations and acoustic noise on the cardiac system of the examined persons, which was confirmed by a slight increase in the heart pulse rate and changes in pulse transmission time and pulse wave velocity. We plan to perform further measurements inside the whole-body MRI device producing more intensive vibrations and noise with expected higher stress impact on an exposed person.

Keywords: arterial blood pressure, estimation by linear regression, photoplethysmography signal, pulse transmission time, wearable sensor.

1. INTRODUCTION

The photoplethysmography (PPG) signal consists of a succession of pulse waves (PW), each PW characterizing one heart cycle. We can recognize so called central and peripheral pulse waves, which differ in PW shapes depending on the locations of the PPG signal pick-up on the human body [1], [2]. The typical central wave can be acquired from the carotid artery as a volumetric recording from the skin surface above the vessel. The peripheral pulse wave is picked up from the fingertips of each limb. Clinical studies show that the shape of the peripheral pulse wave of the PPG signal reflects the current state of the human cardiovascular system, including changes in arterial stiffness [3], arterial blood pressure (ABP), and heart rate (HR) [4], [5]. While the term "heart rate" is mostly applied within the context of the electrocardiogram (ECG) signal, a similar parameter calculated from the PPG signal is referred to as "pulse rate" (PR) [6], which will be used throughout this paper. The ABP and HR/PR parameters can be successfully used for stress detection, as they can show some negative physiological and psychological effects on a tested person [7]. It holds also in the case of patient scanning inside the magnetic resonance imaging (MRI) scanner [8]. At present, cardiovascular magnetic resonance imaging is an important imaging technique used for the study of heart structure and function [9]. However, in this type of non-invasive examination device, the pulsating current in the gradient coil system generates mechanical vibration and acoustic noise [10]. Such vibration is often accompanied by a local heating effect, which can be measured by a contactless method using a thermal imaging camera [11]. Contemporary top MRI devices are based on a very high magnetic field of up to 11 T, but low-field MRI scanners are still fully usable [12].

The intensity of vibrations and noise generated in the scanning area of the MRI device depends on several factors. Among them the most important are the design of the scanner device (open-air vs. whole-body), the intensity of the working magnetic field [10] (high/low field devices), and the volume scanned (e.g., MR scan of leg vs. whole human body). Energetic and spectral properties of the generated vibrations and acoustic noise also depend on the type of the scanning sequence used (spin-echo, gradient-echo, high-resolution, 3D, etc.) and its parameters (repetition time, echo time, number of slices, slice orientation and thickness, etc.). These mechanical and acoustic waves affect a person lying on the patient bed in the MRI scanning area. Measurable changes in blood pressure and pulse rate parameters along with other features of a PPG pulse wave can be used to detect and

DOI: 10.2478/msr-2023-0028

Corresponding author: jiri.pribil@savba.sk (J. Přibil)

evaluate this negative effect on the person being scanned. This is particularly important when using the MRI device for 3D modeling of the human vocal tract with simultaneous recording of a phonation signal [13], [14]. The stress induced by the vibration and acoustic noise causes tension in the vocal cords and, in the end, an unwanted modification of suprasegmental and spectral features of the phonation signal, resulting in errors and inaccuracies in the calculation of the 3D models of the vocal tract.

In the long term, we are interested in the analysis of stress in persons scanned in the MRI tomograph operating with a low stationary magnetic field B_0 up to 0.2 T [15], [16]. For stress detection and quantization, we have previously used the PPG signal sampled from a wearable optical sensor on the fingers with parallel measurement of blood pressure values from an external portable blood pressure monitor (BPM) device. However, this type of measurement instrument and set-up is less comfortable for the tested persons, and also presents some practical problems in conducting the whole measurement experiment. The cuff of the BPM device usually contains a metal brace, and the body of the BPM device is not shielded, so it could be damaged when it is used to measure in an environment with a strong radiofrequency (RF) interference. Therefore, our next research aimed to find a cuffless approach [17] to determine ABP values from the PPG signal without using the BPM device.

Our last research [18] focused on an experiment with the application of an indirect approach to estimate systolic (SBP) and diastolic (DBP) arterial blood pressure values from the sensed single PPG wave. The developed method was based on time domain features and pulse areas determined [19] from the second derivative of the PPG signal [20], [17]. In the first step, the database of PPG wave features was created together with blood pressure values measured in parallel by a BPM device (BP_{BPM}). To estimate the ABP values from these features [21], the linear regression method [22] was used to calculate the relation between the parameters determined from the PPG signal and the corresponding BP_{BPM} values. From the performed analysis of correctness and accuracy it is evident that the obtained precision of estimated ABP values depends on the hand used for PPG signal measurement (left/right) and slightly on the gender of the tested person (male/female). The final relative estimation error reached about 7.5% for SBP and 2.6% for DBP values [18]. These results seem to be acceptable for our experiment in the first step, since the typical estimation error of this cuffless method is about $5 \div 10\%$ [20], [17], [23]. On the other hand, it is evident that further refinements are necessary before this method can be used in practice.

To improve the ABP determination precision, the method based on the pulse transit time (PTT) is often used [24]. The PTT generally represents the time difference between ECG and PPG peaks measured in parallel by sensors located at a known distance Dx [25]. Due to a linear relationship between PTT and ABP, the estimation of the blood pressure with PTT is more accurate than with PPG alone (the estimation error decreases to $1.5 \div 5\%$) [26]. However, the ECG signals cannot be measured by a gradient system inside the running MRI device due to the strong RF interference together with a stepwise changed magnetic field. On the other hand, it has been practically confirmed that the signals from the optical PPG sensor can be effectively acquired even from the subject lying in the scanning area of the running MRI device if all parts of a wearable PPG sensor are made of non-ferromagnetic components and are fully shielded [15]. The multichannel reflective PPG sensors have been successfully applied to cancel motion artifacts in wearable reflectance photoplethysmography [27]. In addition, two or more PPG signals picked up simultaneously by sensors on different parts of the hands or legs – typically the wrist and fingers [28] – can be used to determine PTT values. Other parameters, such as pulse wave velocity (PWV) and relative PTT (rPTT), describe the current state of the cardiovascular system of a tested person and are suitable for detecting and evaluating the stress caused by scanning inside the MRI device.

The motivation of this work was to test the applicability of a multi-channel PPG signal sensed inside the open-air low-field MRI device [29] to determine PTT and other pulse wave parameters. This article describes the process of designing, realizing, and testing a special prototype wearable device that includes three optical PPG sensors working in transmittance/reflectance modes with a Bluetooth (BT) wireless connection for real-time data transfer to the recording device. The functionality of the developed sensor was tested under normal laboratory conditions with two PPG signals sensed from one hand at the same time as BP and HR values were measured by the BPM device with its pressure cuff placed on the opposite arm. The obtained time distance parameters were then statistically analyzed to find correlations with the SBP/DBP and PR values obtained from the PPG waves. Finally, the tested subjects lay in the scanning area of the MRI device, and the acquired samples of PPG signals from three optical sensors were wirelessly transmitted to the control device through the shielding metal cage. The practical influence of vibrations and acoustic noise on the cardiac system of the exposed persons was confirmed by slightly increased PR and changed PTT and other analyzed heart pulse transmission parameters (HPTP) determined from the sensed PPG signal.

2. METHODS

While pulse transit time was originally defined as the time difference between ECG and PPG peaks, it can also be determined from PPG signals from optical sensors worn on the wrist and fingers. The real-time algorithm for PTT determination from a multi-channel PPG signal must be fast, stable, sufficiently precise, and relatively easy to implement on the chosen HW platform. The technique used is similar to that used for one-channel PPG signal acquisition [15], [16]. The PPG signals are processed in the following way:

1. For each of the waves (PPG_A, PPG_B, etc.), the signal level threshold L_{THR} is determined to clip them and obtain sequences c_{PPG} of segments of ones (with T_1 samples) and zeros (T_0 samples) corresponding to the input signal above/below L_{THR} (see a demonstration example for a two-channel PPG signal in Fig. 1). The PPG cycle period T_{CP} (in samples) is equal to T_1+T_0 and using the sampling frequency f_s (in Hz) the PR value is calculated as

$$PR = 60 \times f_s / T_{CP} \text{ [min}^{-1}\text{]}. \quad (1)$$

2. The PPG wave typically contains two maxima representing systolic/diastolic peaks. The systolic peak position P_{SYS} can be localized in the middle of each T_1 interval – as documented in Fig. 1. The PTT values are calculated from the differences ΔP_{SYS} (in samples) between the P_{SYS} positions as

$$PTT = \Delta P_{SYS} / f_s \text{ [s]}. \quad (2)$$

3. The pulse wave velocity parameter [30] depends on both the PTT value and on the value of the distance Dx (in m) between locations of the optical PPG sensors

$$PWV = Dx / PTT \text{ [m/s]}. \quad (3)$$

4. The relative percentage parameter rPTT is calculated as the ratio of the PTT value (as ΔP_{SYS} in samples) to the PPG cycle period T_{CP} to be invariant to the current PR value

$$rPTT = (\Delta P_{SYS} / T_{CP}) \times 100 \text{ [\%]}. \quad (4)$$

5. The obtained values are then analyzed and basic statistical parameters (minimum/maximum, mean, and/or variance) are calculated along with histograms of occurrence distributions.

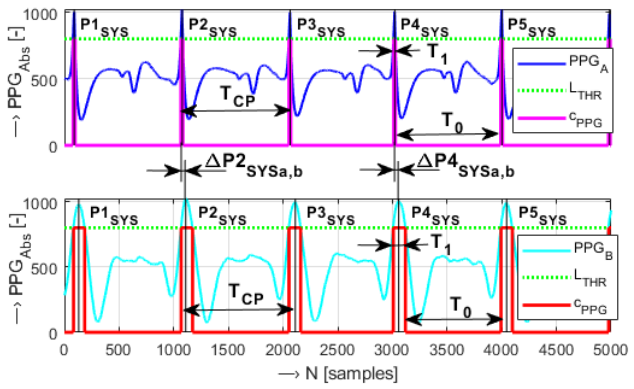

Fig. 1. An example of determining the time differences between systolic pulses $\Delta P_{SYSa,b}$ from the two PPG waves: 5k-sample part of $PPG_{A,B}$ signals together with sequences $c_{PPGa,b}$, with signed cycle periods T_{CP}, lengths T_1, T_0, and localized systolic pulses $P2,4_{SYS}$; $L_{THR} = 800$, $f_s = 1$ kHz.

For the evaluation of partial and summary results of pulse wave parameters, the final representative statistical value H_{FINAL} is always used. The simplest way of H_{FINAL} determination is the calculation of the mean value H_{MEAN}. It often happens that the distribution of the analyzed values has a non-Gaussian character [31]. In this case, the H_{MEAN} value would not give a correct result, so it is better to use the histogram value H_{MAX}, which corresponds to the maximum occurrence O_{MAX} [%]. However, this is valid only in the case of a relatively high O_{MAX}. In case of too small O_{MAX} [%] (below the chosen limit O_{MIN} [%]), the H_{MEAN} value usually gives the result with higher accuracy, but its practical use depends on the second condition, which is based on the absolute difference between the H_{MAX} and H_{MEAN} values: $\Delta H_{DIFF} = |H_{MAX} - H_{MEAN}|$. If ΔH_{DIFF} is less than or equal to the chosen minimum ΔH_{MIN}, the H_{FINAL} value is set to the H_{MEAN} value, otherwise the H_{FINAL} is determined as the median H_{MED} of H_{MAX} and H_{MEAN} values:

$$H_{FINAL} = \begin{cases} H_{MAX} & ; \text{for } O_{MAX} >> O_{MIN} \\ H_{MEAN} & ; \text{for } (O_{MAX} < O_{MIN}) \,\&\, (\Delta H_{DIFF} <= \Delta H_{MIN}) \\ H_{MED} & ; \text{for } (O_{MAX} < O_{MIN}) \,\&\, (\Delta H_{DIFF} > \Delta H_{MIN}) \end{cases}. \quad (5)$$

The graphs in Fig. 2(a), Fig. 2(b) show the obtained values of the differential pulse wave parameters PWV and rPTT, determined from the PPG_{A-B} waves together with the calculated H_{MEAN} values. Fig. 2(c), Fig. 2(d) contain histograms of distribution for these parameters and the values H_{MAX} on the horizontal axes correspond to the maximum occurrence O_{MAX}. The histogram in Fig. 2(c) documents the situation with a non-Gaussian distribution – probably due to local fluctuations in diastolic pulse positions determined from the two-channel PPG signal sensed on one wrist and one index finger. In this case, the maximum occurrence value is relatively high (33.3%), so the value H_{MAX} is used as the H_{FINAL} value. In the histogram in Fig. 2(d), the maximum occurrence O_{MAX} is only 12.2%, so the choice of the value H_{MAX} as a representative value H_{FINAL} is not suitable. Here the difference between the H_{MAX} and H_{MEAN} values is small (below the chosen ΔH_{MIN}), so H_{FINAL} is set to H_{MEAN}.

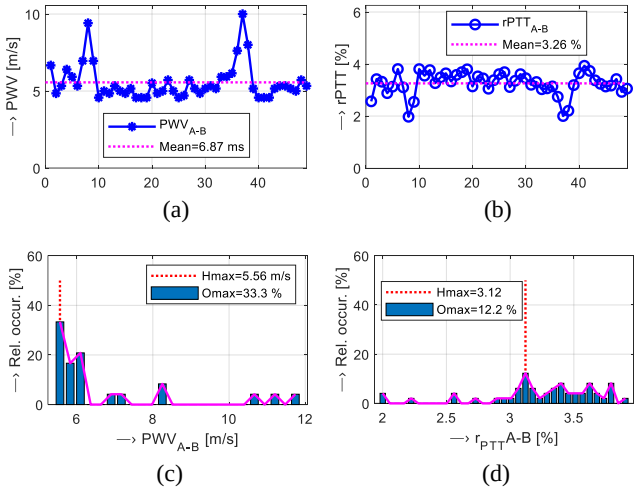

Fig. 2. An example of differential parameters between PPG_A and PPG_B waves together with calculated mean values (upper plots); histograms with marked H_{MAX} at positions of maximum occurrence O_{MAX} (lower plots) for PWV (a), (c) and rPTT (b), (d).

3. Objects, Experiments, and Results

A. *Description of the three-channel wearable PPG sensor*

In agreement with previous developments and realizations of wearable PPG sensors [15], [16], [18], our current prototype consists of similar functional parts:

1. optical pulse sensor(s) for PPG signal pickup,
2. analog interface for PPG signal pre-processing and filtering,
3. microcontroller with a multi-channel A/D converter and a USB interface,
4. wireless (Bluetooth) communication module,
5. power supply by a rechargeable battery or a power bank.

In general, an optical sensor can operate on the transmission or reflection principle. The transmission (TRX) type of a sensor probe usually has a light source (one or more LED elements) and a photo detector placed on opposite sides of the sensed human tissue, and may have the form of a finger ring or clip – this type is often used in oximeters [32]. The reflectance (RFX) type of an optical sensor is mainly attached to the fingers or wrist, typically fixed by an elastic/textile band or integrated as part of wearable devices (fitness bracelets, smart watches, etc.). In this case, the photo detector measures the intensity of light reflected from the skin and is placed on the same side of the skin surface as the light source transmitter.

The current realization of the wearable triple PPG sensor is a relatively simple and low-cost solution, but fully usable for our experimental purposes. It consists of:

- Arduino Nano v.3.3 board based on Atmel processor ATmega328P with f_{CLK} = 16 MHz and eight 10-bit A/D converters [33],
- BT module MLT-BT05 operating with BT4.0 BLE standard at 2.4 GHz,
- Easy Pulse Mikro – a micro Bus compatible pulse sensor with the transmittance PPG optical pulse sensor ER-CDE17527M,
- two reflectance sensors with fully integrated analog interfaces – Crowtail-Pulse Sensor ER-CT010712P (further called “RFX1”) and Pulse Sensor Amped Adafruit 1093 (further called "RFX2”).

For long-term measurement experiments, all components are powered by the AlzaPower Source 2000 mAh 5 V power bank via the USB port. For short-term measurements of PPG signals, it is also possible to use a rechargeable polymer-lithium-ion (Li-Po) cell to power the sensor. The Arduino board, the BT module, and all three optical PPG sensors can operate with a supply voltage in the range from 3.3 V to 5.5 V, and the PPG sensors’ mean DC value in a fully functional state is about 60 mA, so we use the 3.7 V battery cell with a capacity of 1250 mAh. For proper and safe operation in the magnetic field environment, all parts of the PPG sensor are fully shielded in aluminum boxes (see a documentary photo in Fig. 3) and assembled from elements made of non-ferromagnetic materials [15].

The PPG sensor operates in “slave” mode, waiting for commands from the control device to start measuring and sending PPG signal samples received from the optical sensors in real time. The Windows application was built to control multi-channel PPG signal acquisition, processing, and storage on an external master device (laptop). It enables: (1) real-time monitoring and displaying of PPG signals picked up currently from three optical PPG sensors, (2) continuous PPG signal measurement with selected sampling frequency f_s in data blocks of N_{MEAS} samples.

With respect to the type of processor used integrated on the Arduino board, its working clock frequency, and the available memory size, the three-channel parallel measurement can be practically performed in a batch of N_{MEAS} = {1k, 4k, 16k, 32k and 64k} samples. Finally, for the real-time sensing of the PPG signals from all three optical sensors, only the sampling frequencies f_s = {125, 250, 500 Hz, and 1 kHz} can be used. For bi-directional serial BT communication between the triple PPG sensor and the control laptop, the maximum supported baud rate 115200 bps was applied.

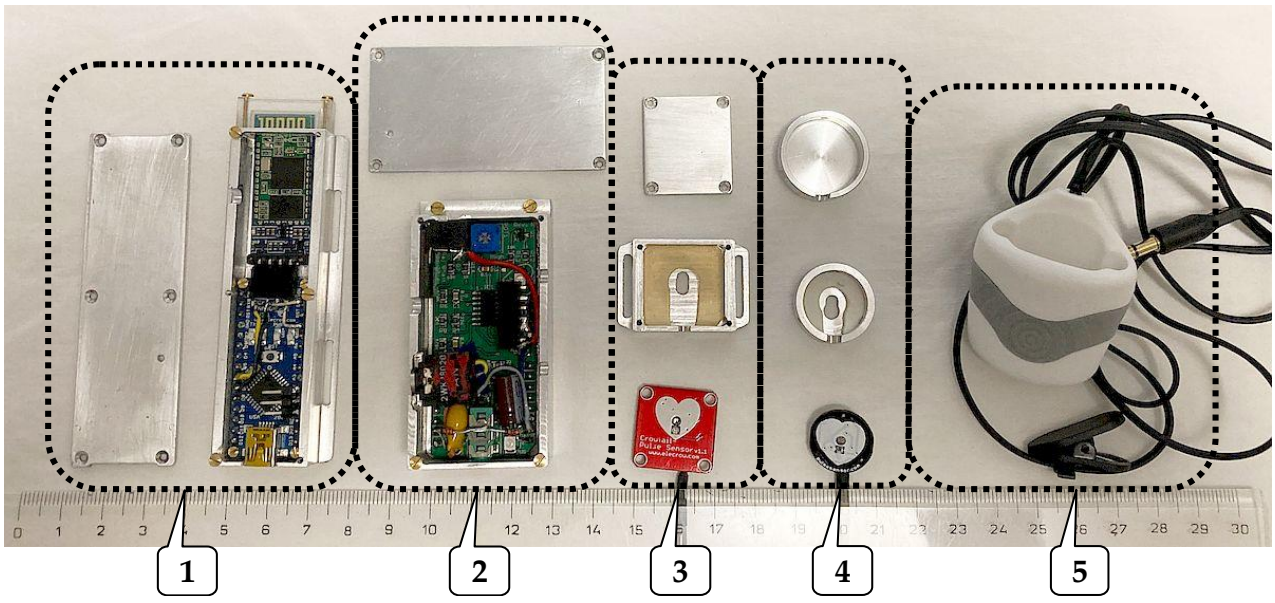

Fig. 3. Assemblage with aluminum covering of the PPGsens-3p sensor: Arduino microcontroller board Nano v.3.3 together with the BT communication module MLT-BT05 (1), analog interface Easy Pulse Mikro (2), reflectance optical sensor ER-CT010712P (3), reflectance optical sensor Adafruit 1093 (4), and transmittance optical pulse sensor ER-CDE17527M (5).

B. Performed measurements and analyses

After testing the functionality of the PPG-3P sensor, including the BT data transmission, two basic types of measurements were performed:

1. sensing of two PPG waves simultaneously with parallel control measurement of the BP and PR values by a BPM device realized under normal laboratory conditions,
2. recording of three-channel PPG signals in a neighborhood and inside of the open-air MRI tomograph operating with a low magnetic field.

In the simultaneous recording of two-channel PPG signals (waves PPG_A and PPG_B), the optical PPG sensors were located as follows: the RFX1 sensor on the wrist artery (W) and the RFX2 sensor worn successively on each finger of the left/right hand (F1,.., F5) to obtain different distances *D*x – as shown in a photo of the principal arrangement in Fig. 4. The body of the developed PPG sensor was laid on the desk together with the power bank for the supply voltage. The distances were measured for each of the tested persons before the PPG signal sensing started. In parallel, SBP/DBP and PR values were measured manually on the opposite hand using the Microlife BP A150-30 AFIB portable BPM device [34].

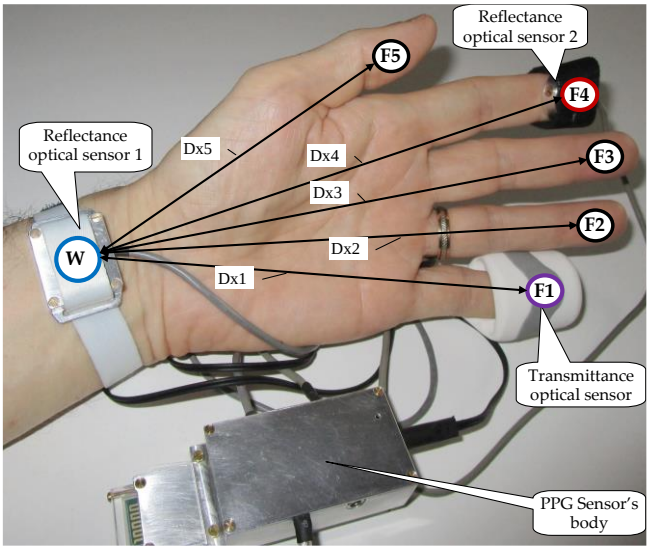

Fig. 4. Principal arrangement of the multiple PPG measurement realized under normal laboratory conditions.

The distances W-F1,..,5 were measured using the estimated positions of the transmission LEDs – see documentary parts (3), (4), and (5) of the photo in Fig. 3. While the *D*x distances are schematically shown by lines in Fig. 4, we actually tried to measure the length of the path between the starting point (wrist W) and the end points (fingers F1-5) along the blood arteries with a flexible meter. The methodology applied derives from the fact that the blood in a measured hand really flows in this way. The measurement was very individual-dependent, so *D*x was finally measured with the maximum accuracy of only 5 mm. To identify consequences of the absolute measurement error of *D*x (AE_{Dx}), the following three auxiliary analyses were performed:

1. determination of basic statistical parameters of *D*x values per finger for both hands of all tested persons, summarized by box-plots in Fig. 5(a),
2. calculation of the relative percentage measurement errors of *D*x (RE_{Dx}) per a finger for U_{Dx} = 5 mm using the minimum, maximum, and mean *D*x distances determined in the previous step – see the graph in Fig. 5(b),
3. simulation of the effect of AE_{Dx} = 5 mm on the relative percentage error of PWV (RE_{PWV}); the investigation was performed for PTT = {15, 25, and 35} ms – see right graph in Fig. 5(c).

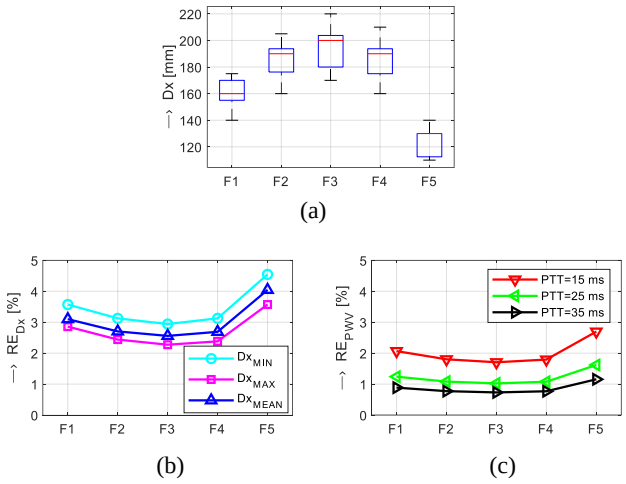

Fig. 5. Visualization of the analysis of the measured distances *D*x for all tested persons: box-plots of basic statistical parameters per finger (a), relative percentage RE_{Dx} errors for {minimum, maximum, and mean} *D*x values (b), relative RE_{PWV} errors for PTT = {15, 25, and 35} ms, using mean *D*x values (c); absolute measurement error of *D*x: AE_{Dx} = 5 mm in all cases.

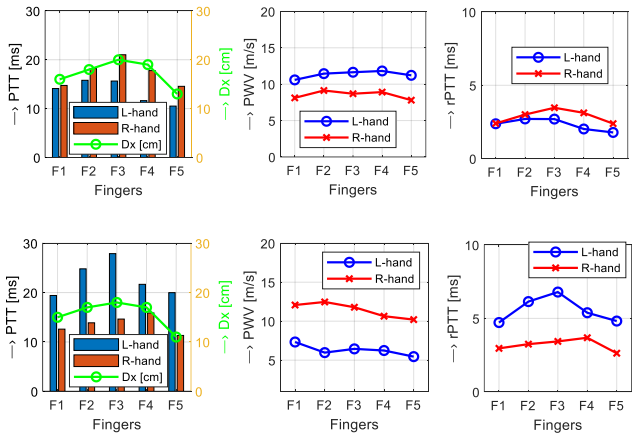

Fig. 6. Comparison of differential parameters between the PPG_A and PPG_B waves for L/R hands of male $P1_M$ (upper plots) and female $P1_F$ (lower plots): PTT values together with measured finger distances *D*x (left), PWV values (middle), and rPTT values (right).

Twelve non-smoker volunteers participated in the first part of the experimental measurements – eight men ($P1\text{-}8_M$) and four women ($P1\text{-}4_F$) with a mean age of 49 ± 15 years. We collected a small database consisting of 120 recordings of

two-channel PPG signals with 64 s duration, sampled at 1 kHz (five records of the left/right hands for each person). The tested person was always sitting with both hands on the table located in the office room; no stimuli were present during the measurement (no conversation, no drinking tea or coffee, etc.).

Selected partial results for $P1_M$ and $P1_F$ tested persons of the PTT, PWV, and rPTT parameters are shown in Fig. 6. Next, Fig. 7 shows a graphical comparison of the resulting mean variance values of HPTPs determined from PPG_A (sensed always at the wrist) and PPG_B waves from different fingers of the left and right hands of all twelve tested persons. Finally, summarized results are presented in Fig. 8, grouped by L/R hands of males/females, consisting of the mutual positions of the parameters PR-PTT, SBP-PWV, and DBP-rPTT, along with their linear fitting.

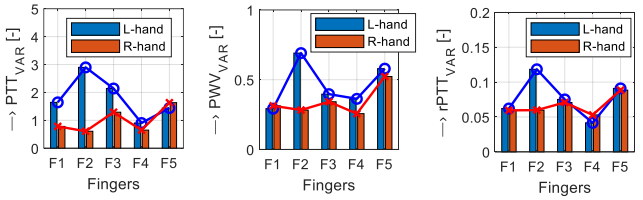

Fig. 7. Resulting mean variance values of HPTPs determined from the PPG_A and PPG_B waves for: PTT (left), PWV (middle), rPTT (right); separately left/right hands, all persons.

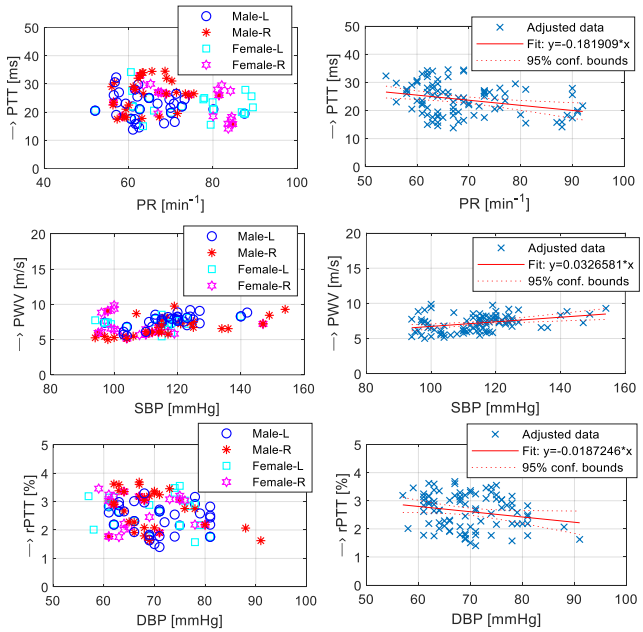

Fig. 8. Mutual positions of the SBP/DBP values measured by the BPM device and HPTPs for all tested persons grouped by L/R hands of males/females (left); fitted by a line segment (right) for: PR-PTT (upper), SBP-PWV (middle), and DBP-rPTT (lower).

The second part of the experiments was performed with the help of the open-air 0.178 T MRI device E-Scan Esaote Opera [29], located in our Institute. The main aim of these measurements can be divided into three basic tasks:

1. testing/verifying the functionality of the developed PPG sensor for parallel three-channel recording of PPG waves in real time and the practical usability of RXF/TXF types of an optical PPG sensor for this task,
2. testing the influence of the real sensing conditions inside the scanning area of the MRI equipment (magnetic field environment with RF interference) on the quality of PPG signals used to determine PTT and other HPTPs,
3. verification and quantification of the observed differences (if any) in the studied HPTPs, determined from the PPG signals sensed inside the ready-but-waiting and the running MRI device.

The measurement experiments were practically performed in the following three phases:

1. *Initialization phase*: The tested person is sitting at a table in the control room outside the metal cover cage of the MRI equipment (further called "Desk"). The optical PPG sensors are attached to the person's left hand. The *D*x distances that were previously measured (within the two-channel experiments) are now checked. After verification of the PPG signal quality and the presence of the time shift between $PPG_{A\text{-}B}$ and $PPG_{A\text{-}C}$ waves for the PTT determination, the body of the whole triple PPG sensor (see the bottom part of Fig. 4) is attached to one arm with an elastic band; the pressure cuff of a portable BPM device is worn on the other arm of the tested person. Finally, the first 64-s frame of the triple PPG signal is sensed and stored together with the parallel measurement of the BP and PR parameters by the control BPM device see the principal measurement schedule in Fig. 9. Both the cuff and the portable BPM device must be removed before the next measuring phase because they contain metal parts that cannot be used for measurement inside the MRI device.

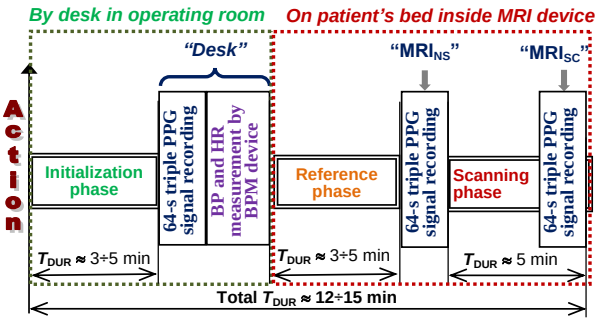

Fig. 9. Principal measurement schedule used in the main PPG signal sensing experiment.

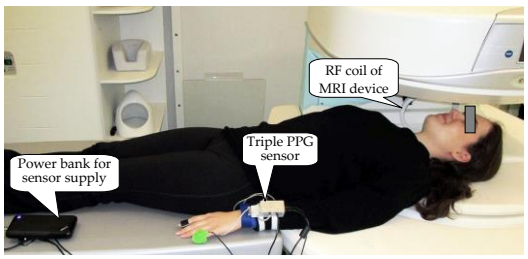

Fig. 10. Photo of a measurement arrangement inside the MRI device E-Scan Opera.

2. *Reference measuring phase*: The tested person, wearing the full triple PPG sensor, moves into the metal shielding cage of the MRI equipment and lies on the patient examination bed (see the arrangement photo in Fig. 10). The MRI device is ready to scan, but no scan sequence is currently executed (this state is further called "MRI_{NS}"). After validating the BT connection through the closed door of the shielding cage and confirming the proper PPG signal quality in the real-time monitoring mode, the second 64-s tree-channel recording of the PPG signal is picked up.
3. *Scanning measuring phase:* The high-resolution MR scan sequence is performed (further called "MRI_{SC}"). The head of the measured subject is situated near the receiving/transmitting RF coil [29] as in our previous experiments [15], [16] to maximize the negative vibration and noise effect on the tested person. The typical time duration of the currently used scan sequence is approximately 5 minutes (including the calibration pre-scan part). During the remaining minute of the MR scanning process, the third 64-s recording of the triple PPG signal is performed.

For all three phases of the parallel triple PPG wave real-time measurements holds that the optical RFX1 sensor was placed on the wrist for sensing of the PPG_A wave, the RFX2 sensor was placed on the index finger (F4) for PPG_B acquisition, and the TRX sensor was placed on the little finger (F1) for pickup of the PPG_C wave. The PPG signal recordings were measured in the 64-k sample data blocks with sampling frequency f_s = 1 kHz. The laptop used to control the PPG measurement was always located outside the shielding cage of the MRI equipment near the operator PC console. The MR scan acquisition and PPG signal sensing were started manually by the experimenter.

The original group of persons measured in the first experiments was reduced by omitting two test subjects (one male and one female) to meet basic safety requirements for persons examined inside the MRI device. Therefore, only seven men ($P1\text{-}6_M$) and three women ($P1\text{-}3_F$) participated in this measurement phase. Partial results of the obtained PTT, PWV, and rPTT parameters determined from the PPG signals sensed under Desk/MRI_{NS}/MRI_{SC} conditions for $P1_M$ and $P4_F$ persons are presented in two sets of bar-graphs in Fig. 11.

Each of the sets is supplemented by a comparison of PR, measured by a BPM (PR_{BPM}), together with BP values and mean PR values determined from the PPG_A wave ($PR_{PPG\text{-}A}$). The final comparison of differences under all three sensing conditions for ten participants is shown by histograms in Fig. 12. These summary results of the occurrence distributions of the studied PTT, PWV, and rPTT parameters are supplemented by a bar-graph comparison of the variances of the $PR_{PPG\text{-}A}$ values. H_{FINAL} values were calculated by the methodology using (5) for all presented results of both parts of the experiments.

The minimum occurrence in the histograms was set to O_{MIN} = 25%, and the limit for the minimum difference between H_{MAX} and H_{MEAN} values was set to ΔH_{MIN} = 20%.

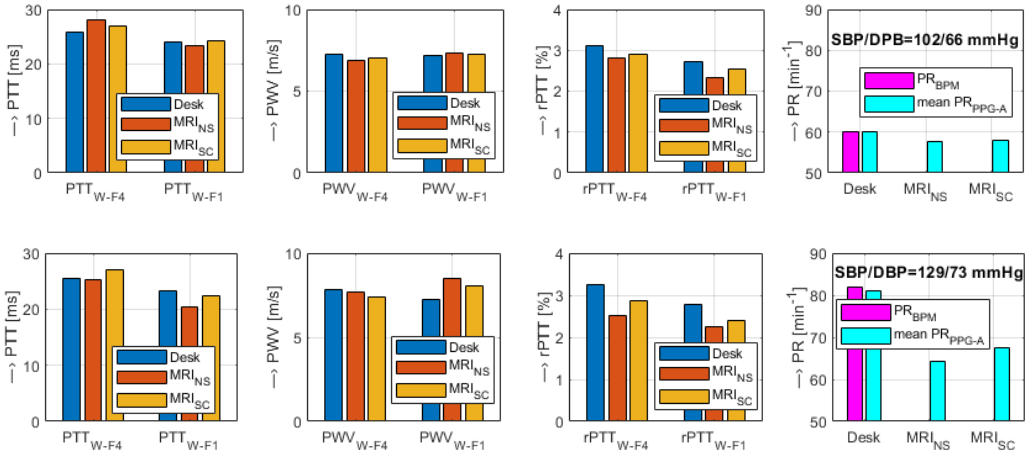

Fig. 11. Partial results of {PTT, PWV, rPTT} parameters determined from the PPG sensed in Desk/MRI_{NS}/MRI_{SC} measuring phases for persons $P1_M$ (upper set), $P4_F$ (lower set) together with PR and SBP/DBP measured by BPM, mean PR calculated from PPG_A.

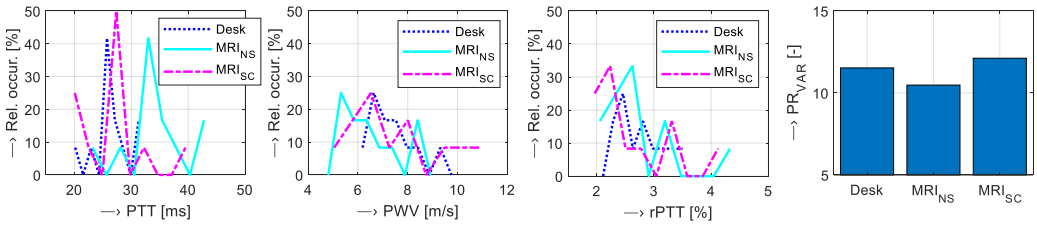

Fig. 12. Histogram comparison of summary results for all participants under Desk and MRI_{NS}/MRI_{SC} PPG signal sensing conditions for {PTT, PWV, rPTT} and bar-graph of the variances of the PR values determined from the PPG_A waves; histograms are calculated from the joint values taken using distances W-F4 and W-F1.

4. DISCUSSION

The first-step measurements verified the functionality of the developed triple PPG sensor both under normal laboratory conditions and in the magnetic field environment with additional radiofrequency and electromagnetic interference inside the running MRI device. The f_s =1 kHz was used to obtain the PPG wave with adequate quality for a correct PTT determination, while f_s = 125 Hz is sufficient for a typical sensing of the PPG signal. For the majority of tested persons, the thumb (finger F5) was too bulky, so the TRX sensor in the form of a rubber ring probe (see the fifth item in Fig. 3) could not be worn there. The summary results for three HPTPs obtained on five tested fingers in Fig. 7 show that their variances depend on the hand measured. This means that the variance of the HPTP parameters is predominantly higher for the left hand, especially in the case of the ring finger (F2), while the lowest variance was obtained for the PPG signals sensed on the index finger (F4). For this reason, the second RFX sensor (for PPG_B sensing) was placed on finger F4 during the second phase of measurements inside the MRI device. As mentioned above, due to practical difficulties, we can measure the *D*x distances with an absolute error of 5 mm. The plots in Fig. 5 document that the highest relative RE_{Dx} errors are in the interval from 3 to 4.5% for the shortest fingers (thumb and little finger) with the minimum measured values of distances W-F1,..,5. The results of the auxiliary analysis show that the inaccuracy of the relative percentage error of the calculated PWV values is detectable, but it has no essential effect on the final precision. The highest RE_{PWV} error of up to 3% was observed for finger F5 at the smallest PTT value of 15 ms. However, this finger is practically not used within the three-channel PPG signal measurements inside the MRI device. Of the fingers used, the maximum RE_{PWV} error at the lowest PPT value was about 2% for finger F1, which can be considered negligible. From the 64-s PPG signal recordings, approximately $60 \div 80$ PPG periods T_{CP} (depending on the current pulse rate) can be detected. The same number of localized systolic peak positions P_{SYS} is sufficient to obtain stable and credible statistical results from the performed analysis.

Partial results of the first measurements under normal laboratory conditions demonstrate that the PWV parameter remains approximately constant for similar values of PR and BP. Graphical comparison in Fig. 6 also confirms visible differences between the results for the left/right hands of both persons (male and female). For both PWV and rPTT parameters, the differences between left and right hands are significantly smaller for the male $P1_M$ person than for the female $P1_F$. In addition, the PTT times obtained for the left hand are approximately twice as high for the $P1_F$ person as for the $P1_M$ person, although both tested persons are right-handed. This may be related to the problem of blood circulation in the $P1_F$ left hand or to the influence of a secondary stress effect during sensing of PPG signals from this hand. The summary graphical results for all tested persons in Fig. 8 show that the obtained mutual positions of the SBP/DBP values measured with the BPM device and the HPTPs can be fitted by a line segment with acceptable slope expressing an ascending or descending trend.

The detailed results for the male $P1_M$ and female $P4_F$ persons, shown in Fig. 11, reveal small absolute differences between the three PPG signal sensing conditions tested. The trend of the changes and the magnitude of the obtained values depend slightly on the pair of PPG waves used to determine the pulse wave parameters (PPG_{A-B} as W-F4 and PPG_{A-C} as W-F1). The differences between the mean PR_{PPG-A} values are also visible in the bar-graphs in Fig. 11. These differences are higher for the PPG signals of the tested woman whose BP and PR_{BPM} were higher in the initial sensing phase.

The final comparison for all persons based on the histograms shown in Fig. 12 shows pronounced maximum occurrence peaks especially for the investigated PTT parameter, where the peak positions for the MRI_{NS} and MRI_{SC} sensing conditions are clearly visible. The maxima obtained for the PWV and rPTT parameters are about half the size, but their positions are still distinguishable. The complemented bar-graph of the variances of the PR_{PPG-A} values shows the expected decrease from the "Desk" to the MRI_{NS} condition, which is affected by a change from the sitting to the lying position of the tested subjects. The MRI_{SC} condition is accompanied again by increased PR variance values caused by sensing of PPG signals during scanning. A relatively high value of PR_{VAR} in the initialization phase "Desk" is surprising. It seems that the mere presence of some people in the operating room of the MRI equipment (with a heavy machine inside a metal cage, the noise of air-conditioning and the automatic calibration system, etc.) has a negative stress effect. This assumption is also supported by the fact that some of the tested persons have significantly higher BP values compared to the measurements in an office room within the first part of the experiments. On the other hand, the monotonous continuous noise generated during the execution of the MR scan sequence, together with a lying position on the patient bed (see the documentary photo in Fig. 10), can sometimes cause drowsiness. For this reason, part of the tested subjects showed a further decrease in the mean PR values (accompanied by a lower variance) in this final phase of PPG signal sensing.

5. CONCLUSION

As mentioned in the Introduction, our long-term research aim is to detect, evaluate, and quantify stress in people undergoing MRI. The main task of our current work, described in this paper, was to test the applicability of a multi-channel PPG signal sensed inside a low-field MRI device to determine PTT and other pulse wave parameters. The results of the experiments performed confirm that this task was accomplished. However, only the practical use of the developed sensor for ABP estimation would show the final estimation error compared to the one obtained in our previous work [18], which was not the aim of the present work. The current experiments were constrained by a limited number of tested persons (the authors and their colleagues), as the IMS SAS does not have approval to study patients in our open-air MRI device designed for standard medical practice, so we can only use it for non-clinical research. In the future, we plan to cooperate with a medical center in Bratislava or in the surrounding area (e.g., Brno, Vienna) that has a certificate for scanning patients with such an MRI device.

In addition to the currently used open-air device, our institute has a whole-body scanner (TMR-96) that can also be used for this type of measurements. The gradient system of the 0.1-T TMR-96 [35] consists of solenoid coils in which stronger currents flow and results in more intensive noise and vibrations with expected higher stress impact on an exposed person. Therefore, we would like to perform more PPG signal measurements inside this device. Finally, we plan to compare the stress effect of these two MRI devices with similar magnetic field from the point of view of their design, and operational and physical parameters.

ACKNOWLEDGMENT

This work was funded by the Slovak Scientific Grant Agency project VEGA2/0004/23 and the Slovak Research and Development Agency project APVV-19-0531.

REFERENCES

[1] Allen, J., Murray, A. (2000). Variability of photoplethysmography peripheral pulse measurements at the ears, thumbs and toes. *IEE Proceedings: Science, Measurement and Technology*, 147 (6), 403-407. https://doi.org/10.1049/ip-smt:20000846

[2] Elgendi, M. (2021). *PPG Signal Analysis: An Introduction Using MATLAB*. CRC Press, 27-36. ISBN 978-1-138-04971-0.

[3] Yousef, Q., Reaz, M. B. I., Ali, M. A. M. (2012). The analysis of PPG morphology: Investigating the effects of aging on arterial compliance. *Measurement Science Review*, 12 (6), 266-271. https://doi.org/10.2478/v10048-012-0036-3

[4] Blazek, V., Venema, B., Leonhardt, S., Blazek, P. (2018). Customized optoelectronic in-ear sensor approaches for unobtrusive continuous monitoring of cardiorespiratory vital signs. *International Journal of Industrial Engineering and Management (IJIEM)*, 9 (4), 197-203. https://doi.org/10.24867/IJIEM-2018-4-197

[5] Nitzan, M., Ovadia-Blechman, Z. (2022). Physical and physiological interpretations of the PPG signal. In *Photoplethysmography: Technology, Signal Analysis, and Applications*. Elsevier, 319-339. ISBN 978-0-12-823374-0. https://doi.org/10.1016/C2020-0-00098-8

[6] Béres, S., Holczer, L., Hejjel, L. (2019). On the minimal adequate sampling frequency of the photoplethysmogram for pulse rate monitoring and heart rate variability analysis in mobile and wearable technology. *Measurement Science Review*, 19 (5), 232-240. https://doi.org/10.2478/msr-2019-0030

[7] Allen, J. (2007). Photoplethysmography and its application in clinical physiological measurement. *Physiological Measurement*, 28 (3), R1-R39. https://doi.org/10.1088/0967-3334/28/3/R01

[8] Celka, P., Charlton, P. H., Farukh, B., Chowienczyk, P., Alastruey, J. (2020). Influence of mental stress on the pulse wave features of photoplethysmograms. *Healthcare Technology Letters*, 7 (1), 7-12. https://doi.org/10.1049/htl.2019.0001

[9] Brablik, J., Ladrova, M., Vilimek, D., Kolarik, J., Kahankova, R., Hanzlikova, P., Nedoma, J., Behbehani, K., Fajkus, M., Vojtisek, L., Martinek, R. (2022). A comparison of alternative approaches to MR cardiac triggering: A pilot study at 3 Tesla. *IEEE Journal of Biomedical and Heath Informatics*, 26 (6), 2594-2605. https://doi.org/10.1109/JBHI.2022.3146707

[10] Moelker, A., Wielopolski, P. A., Pattynama, P. M. T. (2003). Relationship between magnetic field strength and magnetic-resonance-related acoustic noise levels. *Magnetic Resonance Materials in Physics, Biology and Medicine*, 16, 52-55. https://doi.org/10.1007/s10334-003-0005-9

[11] Glowacz, A. (2023). Thermographic fault diagnosis of electrical faults of commutator and induction motors. *Engineering Applications of Artificial Intelligence*, 121, 105962. https://doi.org/10.1016/j.engappai.2023.105962

[12] Marques, J. P., Simons F. J., Webb, A. G. (2019). Low-field MRI: An MR physics perspective. *Journal of Magnetic Resonance Imaging*, 49 (6), 1528-1542. https://doi.org/10.1002/jmri.26637

[13] Schickhofer, L., Malinen, J., Mihaescu, M. (2019). Compressible flow simulations of voiced speech using rigid vocal tract geometries acquired by MRI. *The Journal of the Acoustical Society of America*, 145 (4), 2049-2061. https://doi.org/10.1121/1.5095250

[14] Fischer, J., Abels, T., Özen, A. C., Echternach, M., Richter, B., Bock, M. (2020). Magnetic resonance imaging of the vocal fold oscillations with sub-millisecond temporal resolution. *Magnetic Resonance in Medicine*, 83 (2), 403-411. https://doi.org/10.1002/mrm.27982

[15] Přibil, J., Přibilová, A., Frollo, I. (2020). First-step PPG signal analysis for evaluation of stress induced during scanning in the open-air MRI device. *Sensors*, 20 (12), 3532. https://doi.org/10.3390/s20123532

[16] Přibil, J., Přibilová, A., Frollo, I. (2021). Stress level detection and evaluation from phonation and PPG signals recorded in an open-air MRI device. *Applied Sciences*, 11 (24), 11748. https://doi.org/10.3390/app112411748

[17] Liu, M., Po, L. M., Fu, H. (2017). Cuffless blood pressure estimation based on photoplethysmography signal and its second derivative. *International Journal of Computer Theory and Engineering (IJCTE)*, 9 (3), 202-206. https://doi.org/10.7763/IJCTE.2017.V9.1138

[18] Přibil, J., Přibilová, A., Frollo, I. (2022). Experiment with cuffless estimation of arterial blood pressure from the signal sensed by the optical PPG sensor. *Engineering Proceedings*, 27 (1), 51. https://doi.org/10.3390/ecsa-9-13220

[19] Slapničar, G., Luštrek, M., Marinko, M. (2018). Continuous blood pressure estimation from PPG signal. *Informatica*, 42, 33-42. https://www.informatica.si/index.php/informatica/article/view/2229

[20] Yoon, Y. Z., Yoon, G. W. (2006). Nonconstrained blood pressure measurement by photoplethysmography. *Journal of the Optical Society of Korea*, 10, 91-95. https://opg.optica.org/josk/abstract.cfm?uri=josk-10-2-91

[21] Kachuee, M., Kiani, M. M., Mohammadzade, H., Shabany, M. (2015). Cuff-less high-accuracy calibration-free blood pressure estimation using pulse transit time. In *IEEE International Symposium on Circuits and Systems* (ISCAS). IEEE, 1006-1009. https://doi.org/10.1109/ISCAS.2015.7168806

[22] Rencher, A. C., Schaalje, G. B. (2008). *Linear Models in Statistics*, Second Edition. Wiley, ISBN 978-0-471-75498-5.

[23] Mousavi, S. S., Firouzmand, M., Charmi, M., Hemmati, M., Moghadam, M., Ghorbani, G. (2019). Blood pressure estimation from appropriate and inappropriate PPG signals using a whole-based method. *Biomedical Signal Processing and Control*, 47, 196-206. https://doi.org/10.1016/j.bspc.2018.08.022

[24] Teng, X. F., Zhang, Y. T. (2003). Continuous and noninvasive estimation of arterial blood pressure using a photoplethysmographic approach. In *Proceedings of the 25th Annual International Conference of the IEEE Engineering in Medicine and Biology Society*. IEEE, 3156-3156. https://doi.org/10.1109/IEMBS.2003.1280811

[25] Zhang, J. M., Wei, P. F; Li, Y. (2008). A LabVIEW based measure system for pulse wave transit time. In *2008 International Conference on Information Technology and Applications in Biomedicine*. IEEE, 477-480. https://doi.org/10.1109/ITAB.2008.4570599

[26] Cattivelli, F. S., Garudadri, H. (2009). Noinvasive cuffless estimation of blood pressure from pulse arrival time and heart rate with adaptive calibration. In *6th International Workshop on Wearable and Implantable Body Sensor Networks*. IEEE, 114-119. https://doi.org/10.1109/BSN.2009.35

[27] Wang, L., Lo, B. P., Yang, G. Z. (2007). Multichannel reflective PPG earpiece sensor with passive motion cancellation. *IEEE Transactions on Biomedical Circuits and Systems*, 1 (4), 235-241. https://doi.org/10.1109/TBCAS.2007.910900

[28] Lazazzera, R., Belhaj, Y., Carrault, G. (2019). A new wearable device for blood pressure estimation using photoplethysmogram. *Sensors*, 19 (11), 2557. https://doi.org/10.3390/s19112557

[29] Esaote S.p.A. (2008). *E-scan Opera. Image Quality and Sequences Manual*. 830023522 Rev. A.

[30] Padilla, J., Berjano, E. J., Sáiz, J., Fácila, L., Díaz, P., Mercé, S. (2006). Assessment of relationships between blood pressure, pulse wave velocity and digital volume pulse. In *2006 Computers in Cardiology*. IEEE, 893-896. https://ieeexplore.ieee.org/document/4511996

[31] Lee, C. Y., Lee, Z. J. (2012). A novel algorithm applied to classify unbalanced data. *Applied Soft Computing*, 12, 2481-2485. https://doi.org/10.1016/j.asoc.2012.03.051

[32] Szaj, W., Wojnarowska, W., Pajdo. B. (2021). First evaluation of the PTN-104 plethysmographic sensor for heart rate measurement. *Measurement Science Review*, 21 (5), 117-122. https://doi.org/10.2478/msr-2021-0017

[33] Arduino. *Arduino Nano*. Code A000005 / Barcode 7630049200173.https://store.arduino.cc/products/arduino-nano

[34] Microlife. *Blood pressure monitor BP A150 AFIB*. https://www.microlife.com/support/blood-pressure/bp-a150-afib

[35] Andris, P., Dermek, T., Frollo, I. (2015). Simplified matching and tuning experimental receive coils for low-field NMR measurements. *Measurement*, 64, 29-33. https://doi.org/10.1016/j.measurement.2014.12.035

Received July 04, 2023
Accepted August 22, 2023